Tetraphenylborate Anion Induces Photochromism in N-Salicylideneamino-1-alkylpyridinium Derivatives Through Formation of Tetra-Aryl Boxes

Carletta, Andrea; Colaço, Melwin; Mouchet, Sébastien; Plas, Aurélie; Tumanov, Nikolay; Fusaro, Luca; Champagne, Benoît; Lanners, Steve; Wouters, Johan

Published in:
Journal of Physical Chemistry C: Nanomaterials and interfaces

DOI:
10.1021/acs.jpcc.8b02329

Publication date:
2018

Document Version
Early version, also known as pre-print

Tetraphenylborate Anion Induces Photochromism in *N*-salicylideneamino-1-Alkylpyridinium Derivatives through Formation of Tetra-Aryl Boxes

Andrea Carletta,[1,2] Melwin Colaço,[3] Sébastien R. Mouchet,[1,4,5] Aurélie Plas,[2] Nikolay Tumanov,[1,2] Luca Fusaro,[1] Benoît Champagne,[1] Steve Lanners,[2] and Johan Wouters[1,2]*

[1] Namur Institute of Structured Matter (NISM), University of Namur, 61 rue de Bruxelles, B-5000 Namur, Belgium.

[2] Namur Research Institute for Life Sciences (NARILIS), University of Namur, 61 rue de Bruxelles, B-5000 Namur, Belgium.

[3] Department of Chemistry, St Joseph's College, P O Box 27094, Bangalore 560 027, India

[4] School of Physics, University of Exeter, Stocker Road, Exeter EX4 4QL, United Kingdom

[5] Department of Physics, University of Namur, Rue de Bruxelles 61, B-5000 Namur, Belgium

*Corresponding Author: johan.wouters@unamur.be Tel.: +3281724550

Abstract

N-Salicylideneanilines are interesting model compounds for understanding solid-state photochromism. The introduction of bulky substituents (trityl or *tert*-butyl groups) by chemical modification of the *N*-salicylideneaniline derivative is an effective method to build up photochromic solids. Alternatively, we propose, herein, a supramolecular approach to design photochromic materials which involves the introduction of a bulky anion in the structure. In this context, this is the first report on *N*-salicylideneamino-1-alkylpyridinium salts (iodide and tetraphenylboride salts). Iodide salts were obtained by alkylation of the parent *N*-salicylideneaminopyridine with the appropriate iodoalkane (iodomethane or iodoethane) in acetone. The iodide salts were used as starting material for the production of tetraphenylborate salts by anion-exchange in methanol. All solids were characterized by means of X-ray diffraction and absorption spectroscopy. The effect of different counterions as well as of the crystal structure on the solid-state photochromism is investigated.

Introduction

Photochromism is a color change phenomenon occurring in materials due to reversible transformation of chemical species/molecules/substances following the absorption of electromagnetic radiation.[1–3] Photochromic materials are potential candidates in information storage, optical switching devices and nonlinear optics to name a few.[1–3]

N-salicylideneaniline derivatives are among the most studied thermo- and photo-switchable systems.[4] They can switch between three different colored forms: a colorless enol form, a yellow *cis*-keto form and red *trans*-keto form (**Figure 1**). This color scheme can be affected by both chemical substitution to the chromophore and by the crystal packing. Thermochromism arises from a ground state tautomerization in which the enol form and the *cis*-keto form are involved. Irradiation of the crystalline solid with UV light results in an excited state intramolecular proton transfer (ESIPT) followed by a *cis*-*trans* photoisomerization with final formation of a red-colored *trans*-keto isomer.[5,6] The color transition from pale yellow to red is characteristic of all photochromic *N*-salicylideneanilines.

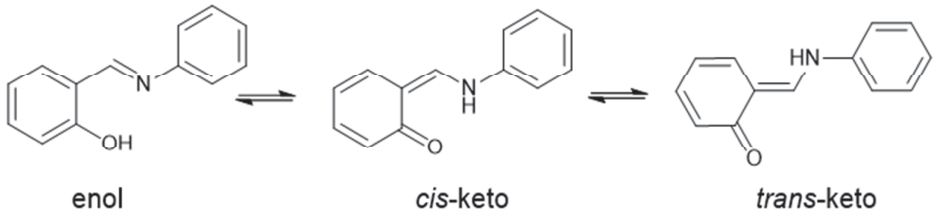

Figure 1. Chemical species involved in photo- and thermochromism of *N*-salicylideneanilines.

Due to steric requirements of the *cis*-*trans* isomerization, photochromism is rarely encountered in the solid state.[4,7] Several works define the concept of open- versus closed-packed structures. Open structures are characterized by molecules in a twisted conformation (with dihedral angle between phenyl rings > 30°) and dominated by edge-to-face interactions. In contrast, closed-packed arrangements are characterized by near-planar molecules stacked with short interplanar distances from 3.3 Å to 3.5 Å.[8,9] It has been suggested that only open-packed arrangements are optimal for photoisomerization to occur (photochromic solids). It has also been shown that the introduction of bulky substituents (trityl or *tert*-butyl groups) by chemical modification[7,10] or introduction of a co-former[11–15] in the crystal structure (salification,[13,16] complexation[17,18] or co-crystallization by hydrogen[9,11] or halogen bonds[14])

are effective methods to build photochromic solids. However, structural factors involved in the expression of photochromism in *N*-salicylideneanilines are not yet understood.[14,19,20]

The use of supramolecular approaches in the design of optical materials[21] is a rapidly growing domain of research.[21–25] By co-crystallization, multiple crystal forms can be built for the same *N*-salicylideneaniline molecule without any need to chemically introduce substituents which could affect the electronic state of the chromophore.[11] Another aspect of this approach is the possibility to obtain isostructural solid forms via the so-called co-former-induced isostructurality.[26–28] Actually, co-crystallization can overcome the functional group dissimilarities that control the crystal packing. Therefore, it can be considered as an efficient tool for the construction of materials having the same architecture (isostructural) but with systematically tunable properties (punctual modifications).[29–31] Studying the photochromic behavior of molecules embedded in highly similar environments, as it happens in isostructural co-crystals, could provide insights on factors that determine photochromism.[14]

A last advantage of co-crystallization, which is a direct consequence of the induced isostructurality, is the possibility to prepare solid solutions[32] of the chromophores (**Figure 2**). The substances may be soluble over a broad range of relative concentrations,[33,34] producing a crystalline solid with properties varying continuously over this concentration range[33,34] or which shows characteristics of the two (or more) combined substances.[35]

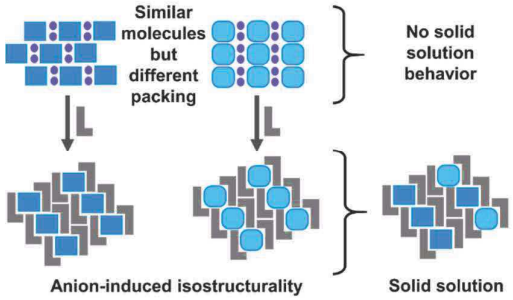

Figure 2. Anion-induced isostructurality and solid solution behavior triggered in the newly obtained isostructural multicomponent systems (purple circle = small anion, L-shaped grey object = bulky anion, blue rectangle = cation **1**, light blue rounded rectangle = cation **2**).

In this context, we study the effects of crystal structure and counteranion size on the solid-state photochromism in some example of *N*-salicylideneamino-1-alkylpyridinium salts (iodide and tetraphenylboride salts). Iodide salts were obtained by alkylation of the parent *N*-salicylideneaminopyridine using the appropriate iodoalkane (iodomethane for **1**, and iodoethane for **2**) in acetone. The iodide salts, **1** and **2**, were used as starting material to prepare the bulky tetraphenylborate salts **3** (from **1**) and **4** (from **2**) by anion-exchange in

methanol (**Figure 3**). Salts **3** and **4** were mixed in a solid solution of $\mathbf{3}_{0.62}$-$\mathbf{4}_{0.38}$ type isostructural to the starting salts **3** and **4**.

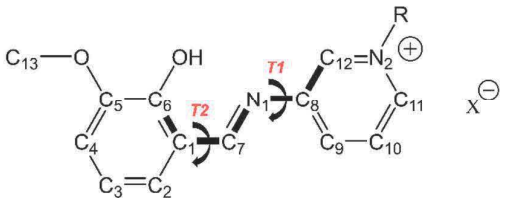

Figure 3. Chemical diagram and numbering scheme of salts under study (**1**: R = Me, X= I. **2**: R = Et, X= I. **3**: R = Me, X= BPh_4. **4**: R = Et, X= BPh_4). Torsion angles, discussed in the text, are **T1**: C_6-C_1-C_7-N_1 and **T2**: C_7-N_1-C_8-C_{12}. Dihedral angle between the two aromatic rings is labelled as **Φ** (not shown in the figure)**.**

Experimental Methods

Materials. *ortho*-Vanillin (*2-hydroxy-3-methoxybenzaldehyde*), 3-aminopyridine, iodomethane and iodoethane were purchased from Sigma-Aldrich and used as received. Solvents used for synthesis and crystallization (MeOH, acetone and acetonitrile from Acros Organic Geel, Belgium) are commercially available and were used without further purification.

Synthesis of the compounds

(E)-2-Methoxy-6-(pyridin-3-yliminomethyl)phenol was synthesized by mechanochemical synthesis[11,36] following a procedure reported earlier.[37,38] Dry grinding was performed in a 2 mL Eppendorf tube using a Retsch MM 400 Mixer Mill.

Synthesis of 1. 3-{(E)-[(2-Hydroxy-3-methoxyphenyl)methylidene]amino}-1-methylpyridin-1-ium iodide. (E)-2-Methoxy-6-(pyridin-3-yliminomethyl)phenol ($C_{13}H_{12}N_2O_2$, 0.8 g) was dissolved in acetone (16 mL) under stirring. Subsequently, iodomethane (261 μL) was added dropwise to the solution and the reaction mixture was stirred overnight at room temperature. A yellowish-orange solid was obtained, recovered by filtration and washed with acetone. Yield: 86 %. The recovered solid was analyzed by powder X-ray diffraction. Its powder pattern matched with the one calculated from the single-crystal structure of **1** (**Figure S1**). Prisms of compound **1**, suitable for single-crystal X-ray diffraction, were obtained by slow evaporation from a saturated solution in acetonitrile after 4 days. Crystals were found to be dichroic, *i.e* they exhibit two different colors (yellow and red in this particular case) when observed at different angles (especially with polarized light).

Synthesis of 2. 1-Ethyl-3-{(E)-[(2-hydroxy-3-methoxyphenyl)methylidene]amino}pyridin-1-ium iodide. (E)-2-Methoxy-6-(pyridin-3-yliminomethyl)phenol ($C_{13}H_{12}N_2O_2$, 0.8 g) was dissolved in acetone (16 mL) under stirring. Iodoethane (336 μL) was then added dropwise to the solution and the reaction mixture was stirred overnight at room temperature. A yellowish-orange solid was recovered by filtration and washed with acetone. Yield: 75 %. The recovered solid was analyzed by powder X-ray diffraction. Its powder pattern matched with the one simulated from the single-crystal structure (**Figure S1**) of **2**. Orange needles of compound **2**, suitable for single-crystal X-ray diffraction, were obtained by slow evaporation from a saturated solution in ethyl acetate after 3 days.

Synthesis of 3. 3-[(E)-[(2-Hydroxy-3-methoxyphenyl)methylidene]amino]-1-methylpyridin-1-ium tetraphenylborate. A stoichiometric amount of $NaBPh_4$ was added to a solution of 50 mg of **1** in 4 mL of methanol. The solution was warmed until complete dissolution was achieved and then kept at room temperature to form a yellow precipitate of **3**. This yellow product was filtered, washed in MeOH and dried under vacuum.

Comparison of the diffractogram of the ground powder, taken directly after synthesis, with the one calculated from single-crystal data for **3**, confirms selective formation of solid **3** (**Figure S1**). Single crystals suitable for X-ray analysis were obtained by slow evaporation of saturated solutions in MeOH after 4 days.

Synthesis of 4. 1-Ethyl-3-[(E)-[(2-hydroxy-3-methoxyphenyl)methylidene]amino]pyridin-1-ium tetraphenylborate. A stoichiometric amount of $NaBPh_4$ was added to a solution of 50 mg of **2** in 4 mL of MeOH. The solution was warmed until complete dissolution was achieved. This solution was kept at room temperature to form a precipitate of **4**. This yellow product obtained was filtered, washed in MeOH and dried under vacuum.

Comparison of the powder pattern, of the as-synthesized product, with the calculated diffractogram from single-crystal data of **4** (see the structural characterization section), reveals selective formation of solid **4** (**Figure S1**).

Synthesis of $\mathbf{3_{0.62}}$-$\mathbf{4_{0.38}}$ solid solutions. Equimolar quantities of **3** and **4** were dissolved in ethyl acetate. Crystals of $\mathbf{3_{0.62}}$-$\mathbf{4_{0.38}}$ suitable for X-ray analysis were obtained by slow evaporation of solvent at room temperature after 2 days.

Characterization

Single-crystal X-ray diffraction. Single-crystal diffraction data for **1**-**4** and $\mathbf{3_{0.62}}$-$\mathbf{4_{0.38}}$ were collected at 20 °C on an Oxford Diffraction Gemini Ultra R system (4-circle kappa platform, Ruby CCD detector) using Mo Kα (λ = 0.71073 Å) radiation for **1**-**3** and Cu Kα (λ = 1.54184

Å) for **4** and $\mathbf{3_{0.62}}$-$\mathbf{4_{0.38}}$. The structures were solved by SHELXT[39] and then refined by full-matrix least square refinement of $|F|^2$ using SHELXL-2016.[40] Non-hydrogen atoms were refined anisotropically; hydrogen atoms (except those bounded to disordered atoms) were located from difference Fourier map. Hydrogen atoms non-involved in hydrogen bonding were refined in the riding mode with isotropic temperature factors fixed at $1.2U_{eq}$ of the parent atoms ($1.5U_{eq}$ for methyl group). Coordinates of the hydrogen atoms implicated in hydrogen bonds were refined. Static positional disorder in the pyridine moiety of crystalline **3** (due to simultaneous presence of two near-equally plausible conformations, **Figure S2**) was refined with 0.78 : 0.22 occupancies ratio. Similar disorder was detected for **4** and $\mathbf{3_{0.62}}$-$\mathbf{4_{0.38}}$, but only for one chromophore ion in the asymmetric unit and occupancy of the minor component was ~6%. However, inclusion of this disorder in the refinement does not improve significantly the refinement while requiring many parameters, so we decide not to include it in the final refinement. Substitutional disorder (methyl/ethyl group) was refined in the $\mathbf{3_{0.62}}$-$\mathbf{4_{0.38}}$. The initially occupancies ratio obtained from the refinement was close to the one from NMR data, but refinement was not stable, so occupancies ratio was fixed to 0.62 : 0.38. The program Mercury[41] was used for molecular graphics.

Powder X-ray Diffraction Measurements. X-ray powder patterns (Cu Kα radiation, step size 0.017°; 45 mA, 30 kV) were collected in the 2θ range 5-40° using a Panalytical X'Pert PRO diffractometer (Bragg-Brentano geometry, X'Celerator detector). The program Mercury was used for calculation of X-ray powder patterns from single crystal data.

UV-Vis diffuse reflectance. Measurements were performed on pure powder samples. Reflectance spectra of solid samples were acquired with a Varian 5E spectrophotometer equipped with a "praying mantis" diffuse reflection accessory and was converted to absorption spectra using the Kubelka–Munk function.[42] Photochromism investigations were performed by irradiating powder samples by using a MAX-303 lamp (Xenon light source 300W) at 360 nm (by use of 20 nm bandpass filters). Thermal fading was analyzed by monitoring the evolution of absorption at 500 nm (Spectra measured each 10 min over 1200 min, in a dark environment).

NMR Spectroscopy. The proton NMR spectra were collected on a Varian VNMRS 400 MHz NMR spectrometer operating at 25 °C. Quantitative ^{1}H NMR spectra were recorded using an excitation pulse of 90° and a recycle delay equal to 10.0 s (maximum longitudinal relaxation time = 2.0 s). The ^{1}H chemical shifts were calibrated using the residual signal of DMSO (2.50 ppm). After the single crystal X-ray diffraction experiment, a single crystal of the solid solution $\mathbf{3_x4_{(1-x)}}$ was transferred in a coaxial NMR tube and dissolved in deuterated DMSO. The composition of

crystals of $\mathbf{3}_x\mathbf{4}_{(1-x)}$ was therefore determined by NMR spectroscopy. The NMR spectrum shows only peaks that are characteristic of ions **3** and **4** (and of the tetraphenylborate anion). By integrating the area underneath those peaks, the relative ratio of **3** and **4** in $\mathbf{3}_x\mathbf{4}_{(1-x)}$ was determined quantitatively. Solid solution composition is of type $\mathbf{3}_{0.62}$-$\mathbf{4}_{0.38}$. The same composition was found for polycrystalline powders used for UV-Vis diffuse reflectance.

When DMSO is used, the enol tautomeric form is the one detected.

Micro-spectrophotometry. The UV-Vis transmission spectra of a single crystal of **1** were acquired using a conventional optical microscope (OLYMPUS BX61) in transmission mode equipped with an optical fiber connected to a spectrophotometer (Ocean Optics USB4000). A polarized white light source was used for each measurement and the analyzer was removed. A total of 13 spectra were acquired on single crystals of **1**, to study its dichroic behavior, by moving the polarizer from 0° to 180° by 15° steps (integration time of 500 ms averaged over 5 scans).

Results and Discussion

Structural Characterization

The aim of this structural characterization section is to find common structure features and to correlate them with the expression of photochromism in the systems under study. The crystal packing features of **1-4** are discussed below (see **Table S1** and **S2** for crystallographic parameters). This is accompanied by an analysis of the **T1** and **T2** torsion angles and of the **Φ** angle defined in **Figure 3**. The **T2** angle is close to 0° in all derivatives due to the intramolecular hydrogen bond involving the –OH group and the imino group. **T1** and **Φ** have been indicated as descriptors of the likelihood of solid-state photochromism in previous works. Specifically, it was stated that photochromism is preferentially encountered for **T1** > 25° and/or **Φ >** 30°. The twisted conformation resulting from **T1** values greater than 25° (or **Φ >** 30°) should account for an open crystal packing which should be required for photochromism.[4,7,43] However, several workers have shown the limits of this prediction rule both in single-component and multi-component crystal systems (co-crystals, salts, solvates).[4,9,11,14,18,44] Nevetheless, for the sake of completeness, values of **Φ** are provided in the structure analysis (values of **T2** and **T1** are provided in **Table S3**).

Compound 1. Compound **1** crystallizes in the $P2_1/c$ space group. The tautomeric form observed under the experimental conditions is the enol form, as deduced from selected bond lengths (**Table S4**) and hydrogen position. Ions of **1** present a near-flat conformation with

calculated value of **Φ** of about 1.9(2)°. Piles of stacked centrosymmetric dimers (head-to-tail stacking) propagate along the *b*-axis. Adjacent piles are symmetrically related by 2-fold screw axes running parallel to the piles. The resulting crystal packing assumes a *herringbone* feature[45] when viewed along the *c*-axis (**Figure 4**).

Compound 2. Compound **2** crystallizes in the $P2_1/c$ space group. The only tautomeric form detected under the experimental conditions is the enol form. **T2** torsion angle is constrained by an intramolecular H-bond to a near-planar value. The overall conformation of the chromophore is planar and described by **Φ** = 2.1(2)°. A head-to-tail stacking between chromophore ions is present as for **1**. The stacked centrosymmetric dimers propagate along the *a*-axis. However, the resulting crystal packing shows a *layered* aspect when viewed along the crystallographic *b*- and *c*-axis (**Figure 4**).

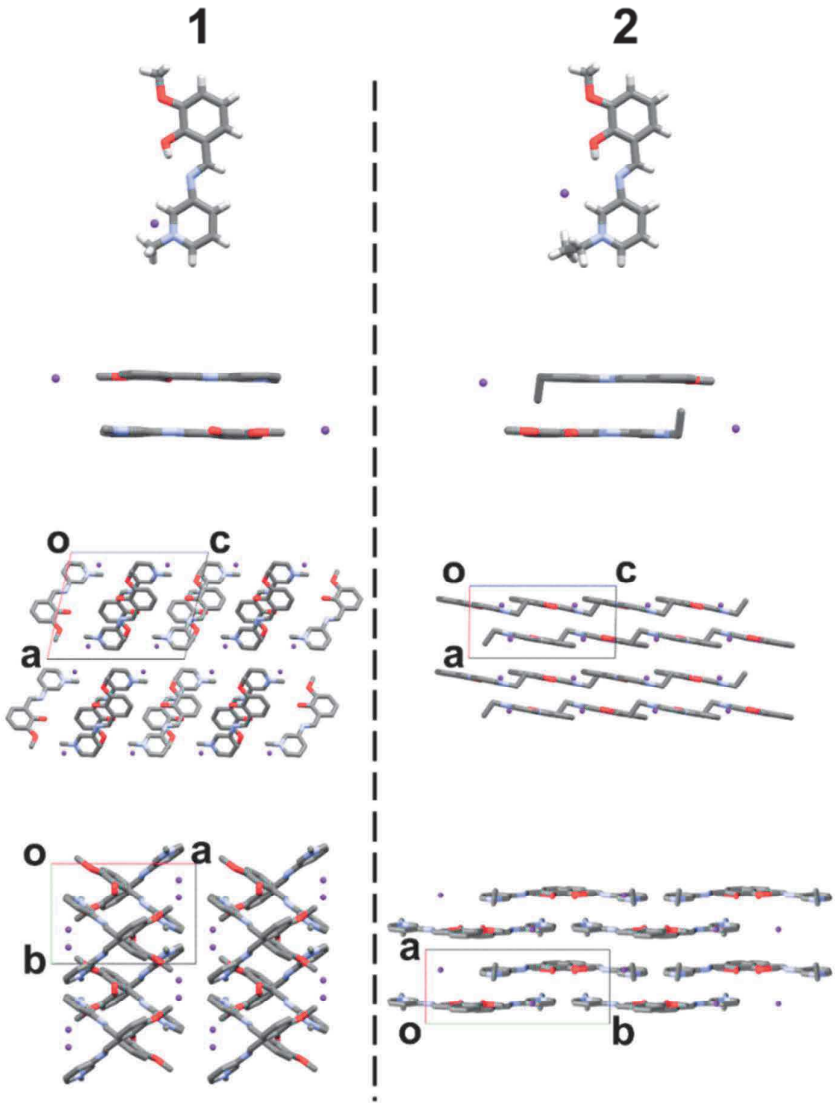

Figure 4. Asymmetric unit of **1** (left) and **2** (right) along with the head-to tail dimers and view along the *b*- and *c*-axis (from top to bottom).

Compound 3. Compound **3** crystallizes in the $P2_1/n$ space group with one chromophore and one tetraphenylborate in the asymmetric unit.

The only tautomeric form detected under the experimental conditions is the enol form. The methylpyridinium moiety, of the *N*-salicylideneamino-1-alkylpyridinium derivative in crystalline **3,** is affected by a static positional disorder due to simultaneous presence of two near-equally plausible conformations. The two conformers present a non-planar conformation tilted by a **Φ** angle of about 42.5(3)° and 44.3(3)° in the disordered moiety (**Figure S2**). Introduction of bulky anions in the structure disrupts the head-to-tail stacking observed in **1** and **2**. Two tetraphenylborate anions interact, through their phenyl groups, with the methylpyridinium moiety of the chromophore resulting in a cage-like assembly (tetra-aryl box) held by π…π stacking and electrostatic interactions. The vanillidene moiety is outside of the cage but partially hindered by the tetraphenylborate anions for interactions with other chromophore ions. The only detected interactions directed to the vanillidene moiety are weak orthogonal C—H…O contacts (see **Figure 5**). In principle, one half of the chromophore is strongly bound whereas a second half is only weakly bound.

Compound 4. Compound **4** crystallizes in the triclinic $P\bar{1}$ space group with two ions of chromophore and two of tetraphenylborate in the asymmetric unit. Despite belonging to a different space group, solids **3** and **4** are isostructural (see **Figure 5** for structure overlap, and **Figure S1**).[46] The ethyl group acts by slightly deforming the structure, a factor which leads to decrease of symmetry (see **Table 1**). The only tautomeric form detected under the experimental conditions is the enol form. The two crystallographically independent chromophore ions show **Φ** of 37.6(2)° and 48.6(3)°, respectively (see **Table S1**).

Solid solution $3_{0.62}$-$4_{0.38}$. Solid $\mathbf{3_{0.62}}$-$\mathbf{4_{0.38}}$ crystallizes in the triclinic $P\bar{1}$ space group with two ions of chromophore and two of tetraphenylborate in the asymmetric unit (**Figure S3**).

Dihedral **Φ** angle for the two crystallographically independent chromophores is 39.2(3)° and 44.6(3)° (see **Table S2**).

This solid solution is isostructural to the starting solids **3** and **4** as confirmed by analysis of unit cell parameters (see **Table 1**). One should take into account that β angle of **3** is supplementary to the one of **4** and $\mathbf{3_{0.62}}$-$\mathbf{4_{0.38}}$, so they are different only due to unit cell choice conventions for triclinic and monoclinic systems (see **Table 1**). The $\mathbf{3_{0.62}}$-$\mathbf{4_{0.38}}$ solid solution obeys Vegard's law: a linear relation exists between the unit cell volume of the solid solution

and the concentrations of the constituent elements, *i.e.* **3** and **4**.[47] Calculated composition from Vegard's law is of 0.60 : 0.40, which is very close to values obtained by NMR experiment.

Table 1. Cell parameters of **3**, **4** and $\mathbf{3_{0.62}\text{-}4_{0.38}}$

	3	$\mathbf{3_{0.62}\text{-}4_{0.38}}$	**4**
Space group	$P2_1/n$	$P\bar{1}$	$P\bar{1}$
a (Å)	11.2697(2)	11.2975(2)	11.3269(3)
b (Å)	16.2411(2)	16.5277(2)	16.7355(5)
c (Å)	17.4036(3)	17.3521(3)	17.4740(5)
α (°)	90	89.2858(12)	89.396(2)
β (°)	104.2390(18)	75.1350(15)	74.793(3)
γ (°)	90	88.9588(13)	88.828(2)
V (Å^3)	3087.56(9)	3130.96(9)	3195.71(17)

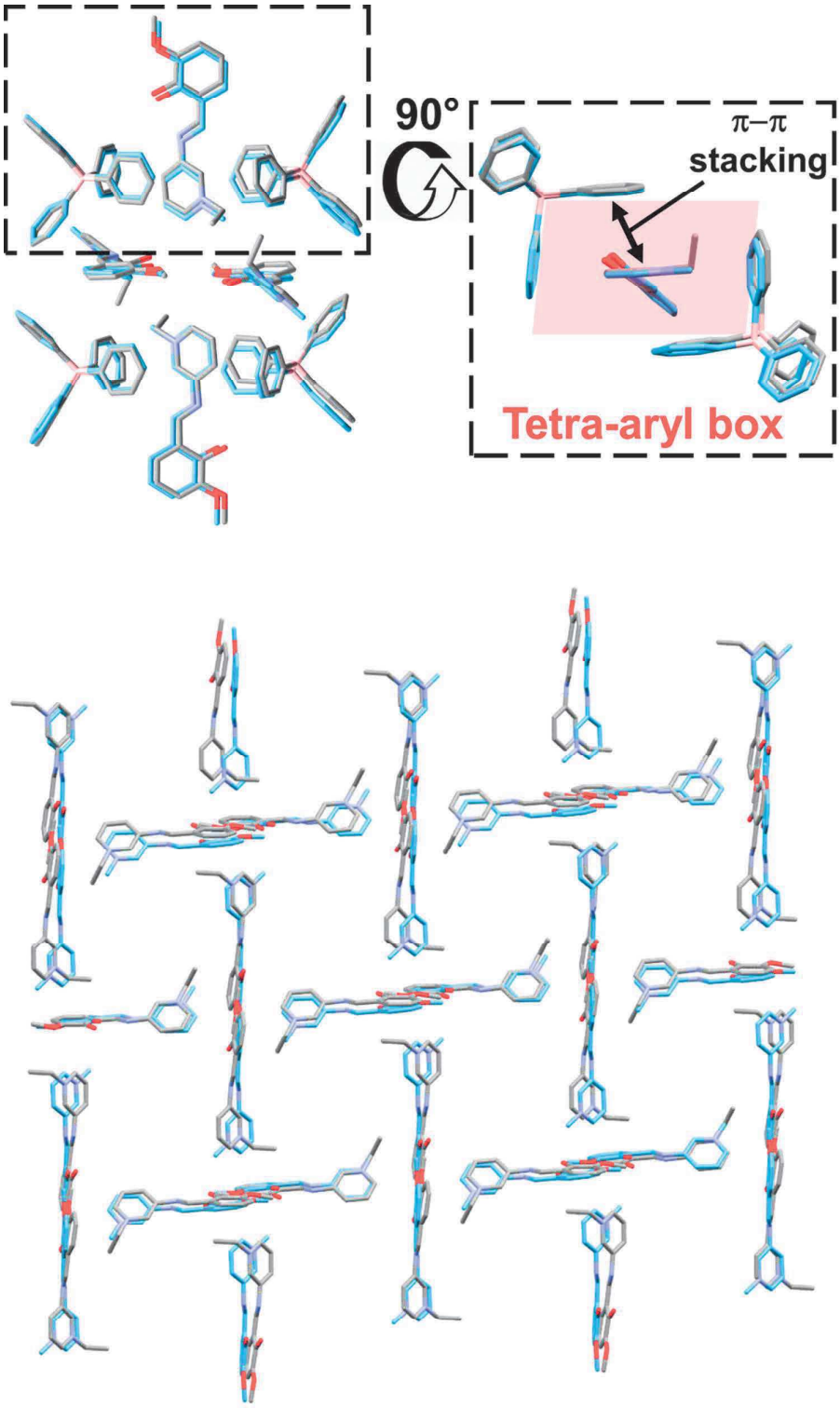

Figure 5. Superimposed crystal structures of **3** (blue) and **4** (grey). An 8-membered supramolecular assembly (top left). View of a tetra-aryl box highlighted by a red area (top right). Overview of chromophores orthogonal arrangement in **3** and **4** by omitting the tetraphenylborate anions. Hydrogen atoms and disorder (in **3**) have been omitted for clarity.

Attempts to obtain a solid solution of $\mathbf{1}_x\mathbf{2}_{(x-1)}$ type have so far been unsuccessful. In fact, it has been shown how an ethyl (solid **2**) in place of a methyl (solid **1**) substitution dramatically changes the structure from a *herringbone* arrangement to a *layered* one in solids **1** and **2**. The lack of isostructurality suggests that the protruding ethyl group (of **2**) cannot be fitted in the compact structure of **1**. This is the main reason for which a $\mathbf{1}_x\mathbf{2}_{(x-1)}$ solid solution could not be obtained.

Instead, in structures **3** and **4**, the tetra-aryl box[48] (**Figure 5**) formed by two bulky anions represents a loose region of the crystal packing where the protruding ethyl group can be accommodated without significant steric strain. In other words, the tetra-aryl box "hides" the protruding alkyl group (methyl or ethyl) and the resulting networks are, therefore, isostructural (**Figure 5**). This case of co-former-induced (or anion-induced) isostructurality suggests that **3** and **4** can generate a solid solution (**Figure 2**).[32] However, it must be pointed out that isostructurality is not a necessary requirement for two molecules to be mixed as long as the flexibility of the crystal packing can compensate steric hindrance and variation of lattice energy.[33,34,49]

Selected distances listed in **Table 2** (centroid labelling in **Figure 6**) confirm this structural flexibility showing that the ethyl group acts by slightly opening the tetra-aryl boxes and by slightly increasing the distance between chromophore ions. This aspect is corroborated by analysis of the structural parameters of the $\mathbf{3}_{0.62}\mathbf{4}_{0.38}$ which show values intermediate between those of **3** and **4.**

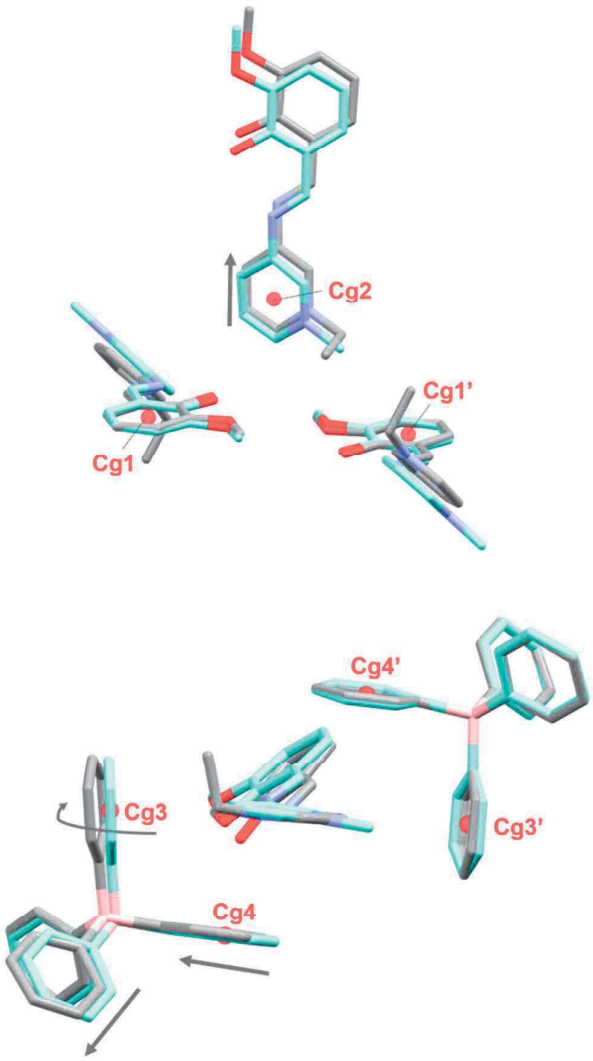

Figure 6. Centroids labelling (Selected distances are reported in **Table 2**) adopted in description of **3** (blue sticks), **4** (grey sticks) and their solid solution $\mathbf{3}_{0.62}\mathbf{4}_{0.38}$ (not shown). Hydrogen and disorder (in **3**) are omitted for clarity. Arrows show the shift in the structure from **3** to **4**.

Table 2. Selected distances in structures **3**, **4**, and their solid solution $\mathbf{3}_{0.62}\mathbf{4}_{0.38}$ (centroids labelling is provided in **Figure 6**).

Distance (Å)	3	$3_{0.62}4_{0.38}$			4
Cg1…Cg1'	8.500(4)	8.497(4)	8.560(3)	8.540(3)	8.560(3)
Cg1…Cg2	5.790(4)	5.797(3)	5.838(3)	5.795(3)	5.962(4)
Cg3…Cg3'	9.971(3)	9.994(3)	10.157(3)	10.157(3)	10.394(3)
Cg4…Cg4'	7.845(3)	7.792(3)	7.929(3)	7.922(3)	7.908(3)
B1…B1'	11.498(3)	11.404(3)	11.694(3)	11.579(3)	11.739(3)

Photochromism and thermochromism

The photochromic behavior of powder samples of compounds **1**-**4** was investigated by irradiating the samples at 365 nm. While irradiation of compounds **1** and **2** did not produce appreciable changes in their Kubelka-Munk (absorption) spectra (**Figure S4** and **S5**), the same experiment for **3** and **4** resulted in significant increase in the 500–600 nm spectral region. The observed variation can be ascribed to the appearance of the absorption contribution of the *trans*-keto tautomer in the 500–600 nm region of the spectrum consistent with a yellow-to-red color change **(Figure S4** and **S5**). Therefore, only **3** and **4** present a photochromic behavior. From a structural point of view, the non-photochromic character of solids **1** and **2** can be safely ascribed to their closed packing with chromophores arranged in head-to-tail stacked dimers (**Figure 4**) with short interplanar distances (3.278(3) Å for **1** and 3.360(3) Å for **2**). Conversely, mismatching of the structure, due to the tetraphenylborate anions in **3** and **4,** induces disruption of the head-to-tail stacking observed in **1** and **2,** thus facilitating the pedal motion mechanism[6,50] needed for the photoisomerization. Color change can be appreciated by naked eye as shown in **Figure 7**. By leaving **3** and **4** in the dark at RT (**Figure 8**) the red coloration fades over the time as a result of the thermal decay of the *trans*-keto form. This thermal fading process is well described by a bi-exponential decay as has been previously reported (**Figure 8** and **Figure S6-S8**).[7,10,51] Small differences are found in the kinetics of thermal fading processes which reveal that **3** undergoes the slowest process ($\mathbf{t_1}$ = 78.5 ± 1.9 min, $\mathbf{t_2}$ = 470.4 ± 6.9 min) while **4** is of about 1.6 times faster ($\mathbf{t_1}$ = 45.3 ± 0.6 min, $\mathbf{t_2}$ = 476.4 ± 3.2 min). Remarkably, the $\mathbf{3_{0.62}4_{0.38}}$ solid solution is also photochromic and shows a conversion time ($\mathbf{t_1}$ = 55.0 ± 1.7 min, $\mathbf{t_2}$ = 471.2 ± 7.8 min) which is in between that of **3** and **4**. These values corroborate observations based on the crystal structures and show how the ethyl substituent is not directly involved in intermolecular interactions but acts by slightly opening the tetra-aryl boxes of the structure and by slightly increasing distance between chromophore ions which are both favorable factors for the photoisomerization to occur.

It is noteworthy that the thermal decay, and so the photochromic behavior, of the solid solution $\mathbf{3_{0.62}4_{0.38}}$ is closer to the one of **4** although this latter is the minor component of the solid solution. As a matter of fact, although **4** is the minor constituent of the solid solution, 38% of substitution is already enough to decrease symmetry. Therefore, the solid solution crystallizes in the $P\bar{1}$ space group, like solid **4**, rather than in the $P2_1/n$ group, observed for solid **3**. Root mean square deviation (RMSD) was calculated on superimpositions of clusters

of 6 tetraphenylborate ions (number of atoms = 150) in structures **3**, **4**, and solid solution $\mathbf{3}_{0.62}$-$\mathbf{4}_{0.38}$, in order to investigate to which of the two starting solids (**3** and **4**) the solid solution is structurally closer. Value of RMSD is of 0.294 Å for solid solution $\mathbf{3}_{0.62}$-$\mathbf{4}_{0.38}$ related to solid **3** and of 0.166 Å for solid solution $\mathbf{3}_{0.62}$-$\mathbf{4}_{0.38}$ related to solid **4** (**Figure S9**). Even if the three structures can be considered as isostructural, the RMSD values obtained highlight that the solid solution is structurally closer to solid **4** than to solid **3**. This result suggests that it is not the major component that determines the thermal fading behavior but the combined effect that both components together have on the crystal structure.

Microcrystalline powders show moderate (**1** and **2**) and low (**3** and **4**) thermochromism (**Figure S10**).

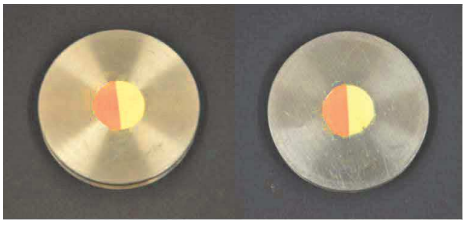

Figure 7. Photochromic color change in powdered form of **3** (left) and **4** (right). Half of the powder was covered by an aluminum foil to avoid exposition to the 365 nm irradiation. The irradiated part, on the left, is orange.

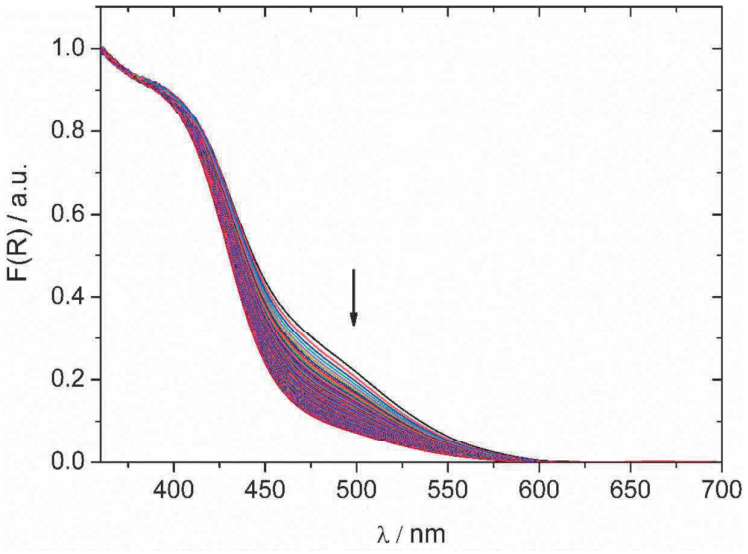

Figure 8. Kubelka-Munk spectra of solid **4** showing the two-steps thermal decay of the *trans*-keto form.

Dichroism of 1

Dichroic materials are characterized by a change in their color when observed at different angles, especially under polarized light. This phenomenon of color change corresponds to a change in their absorptions spectra related to their orientation relative to a source of linearly-polarized light. The absorption of light depends on the relative orientation between molecular transition dipole moment and the direction of polarization of the linearly-polarized light. Light is expected to be most strongly absorbed by the chromophore if these two directions coincide (0° orientation).[52] Dichroic materials can have applications as polarizers, beam splitters or optical filters.[25] The control of dichroism by a crystal engineering[53,54] approach is a new domain of research. A pioneering work on this topic is authored by Bushuyev and co-workers who reported modulation of dichroism by halogen bond co-crystallization of 4,4′-dihalooctafluoroazobenzenes.[25] They concluded that the control over dichroic properties of a material is based on avoiding the formation of *herringbone* structural motifs. Conversely, parallel alignments, like supramolecular chains, lead to highly dichroic materials. Another relevant consequence of a linear (chain) arrangement is that, in principle, dichroism should be observed regardless of the crystal face being chosen.[25] In this context, we studied dichroism in **1-4** (see experimental section for more details). To the best of our knowledge this is the first entry in the literature for *N*-salicylideneamino-1-alkylpyridinium salts derivatives. From a structural point of view, none of the reported solids presents a purely linear arrangement

(chains). Solid **1**, which present a *herringbone* arrangement by looking toward the *c*-axis, showed a strong face-dependent dichroism (**Figure S11-S13**). In particular, $(0\bar{1}1)$ showed a weak color transition from red (darker coloration at 0°) to orange upon 90° rotation of the polarizer (**Figure 9** and **Figure S14**). On the contrary, the color of the $(\bar{1}00)$ crystal face dramatically changes from orange-red to greenish-yellow (**Figure 9** and **Figure S15**). Transmittance spectra quantify the color transition showing a high increase in the 500-600 nm range on changing the linearly-polarized light angle (**Figure 9**). Isostructural, solids **3** and **4** were both found to be non-dichroic, regardless the face being observed. Solid **2** was found to be weakly dichroic (**Figure S16**).

These results are in agreement with reports from literature and show how the *herringbone* packing can lead to nearly perfect isotropic optical properties at certain crystal faces. [53,54]

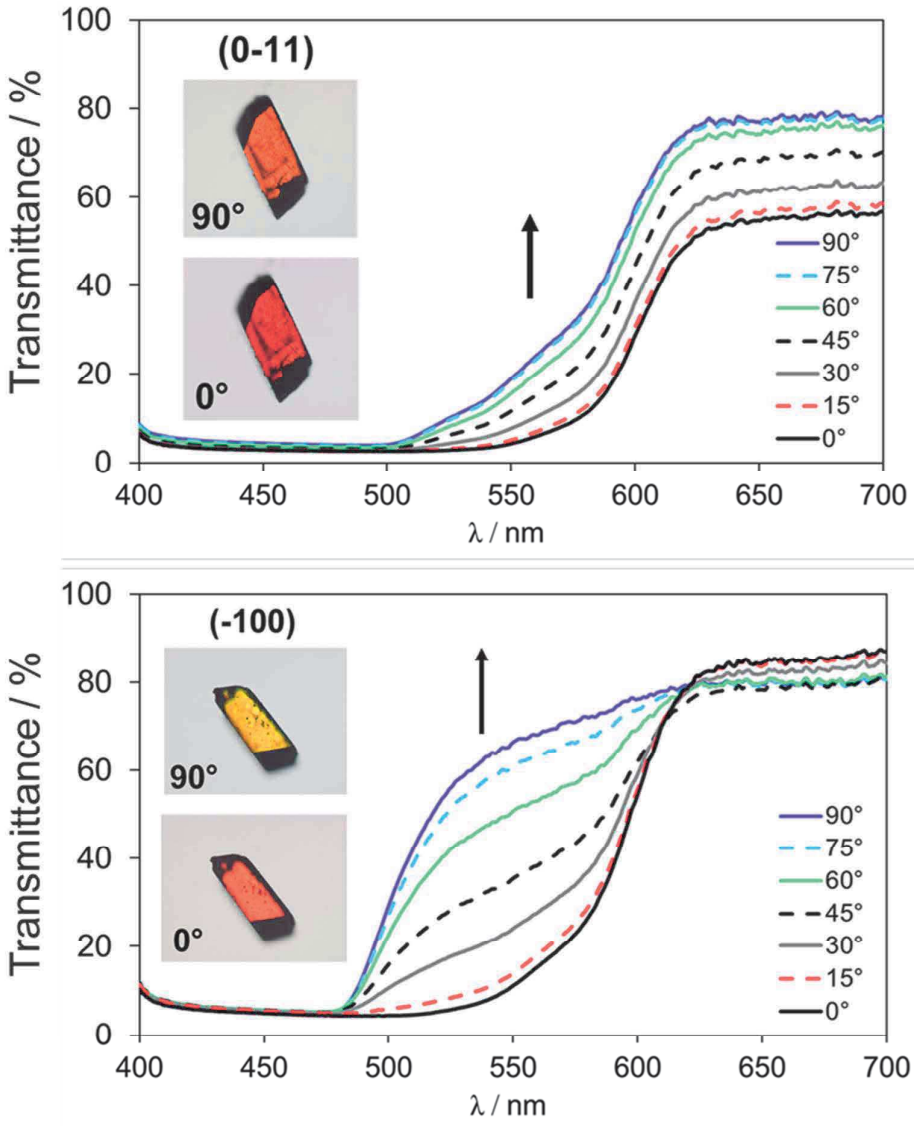

Figure 9. Face-dependent dichroic behaviour of **1** observed on the $(0\bar{1}1)$ crystal face (top) and on the $(\bar{1}00)$ crystal face (bottom).

Conclusions

We have reported here the use of a crystal engineering approach for the construction of photochromic solids based on the use of bulky anions. To the best of our knowledge, this is the first entry in the literature for the *N*-salicylideneamino-1-alkylpyridinium salts (iodide salts, **1** and **2**, and tetraphenylboride salts, **3** and **4**).

We have shown how the small iodine anions (in **1** and **2**) determine formation of highly compact crystal structures. Although, the overall crystal packing of **1** and **2** is different (with the first showing a *herringbone* structure, the latter showing a layered one), both solids are non-photochromic due to the dense packing and to the presence of head-to-tail dimers with short interplanar distances. The replacement of iodide, in **1** and **2**, by the bulky tetraphenylborate anion (solids **3** and **4**) leads to a multiplicity of effects.

First, the resulting solids **3** and **4** are both photochromic due to disruption of head-to-tail stacking structural motifs in non-photochromic compounds **1** and **2**.

Secondly, tetraphenylborate salts, **3** and **4**, are isostructural. This effect, the anion-induced isostructurality, is due to formation of tetra-aryl boxes which permit the accommodation of the alkyl group (methyl for **3** and ethyl for **4**) bound to the pyrimidine moiety of the chromophores, overcoming the molecular differences.

Thirdly, the achieved isostructurality allows **3** and **4** to be mixed in a $\mathbf{3}_{0.62}$-$\mathbf{4}_{0.38}$ solid solution isostructural to the starting salts **3** and **4**. All three isostructural solids (**3**, **4** and $\mathbf{3}_{0.62}$-$\mathbf{4}_{0.38}$) are photochromic confirming the role of crystal structure in determination of photochromism. The study of kinetics of thermal fading reveals that **3** undergoes the slowest process ($\mathbf{t_1}$ = 78.5 ± 1.9 min, $\mathbf{t_2}$ = 470.4 ± 6.9 min) while **4** is of about 1.6 times faster ($\mathbf{t_1}$ = 45.3 ± 0.6 min, $\mathbf{t_2}$ = 476.4 ± 3.2 min). Remarkably, the $\mathbf{3}_{0.62}\mathbf{4}_{0.38}$ solid solution is also photochromic and shows a conversion time ($\mathbf{t_1}$ = 55.0 ± 1.7 min, $\mathbf{t_2}$ = 471.2 ± 7.8 min) which is intermediate between the one of **3** and **4**. This trend is consistent with structure data and shows that the ethyl group acts by slightly opening the tetra-aryl boxes of the structure and by slightly increasing distances between chromophore ions, two favorable factors for photoisomerization.

It is noteworthy that the thermal decay, and so the photochromic behavior, of the solid solution $\mathbf{3}_{0.62}\mathbf{4}_{0.38}$ is closer to the one of **4** although this latter is the minor component of the solid solution. The calculation of RMSD reveals that the solid solution is structurally closer to **4** than **3** even though the former is the minor constituent (38 %). This result suggests that it is not the major component that determines the thermal fading behavior but the combined effect that both components have on the crystal structure.

Microcrystalline powders show moderate (**1** and **2**) and low (**3** and **4**) thermochromism. Dichroism results are in agreement with reports from literature and show how the *herringbone* packing leads to nearly perfect isotropic optical properties at certain crystal faces (face-depended dichroism).

Supporting Information Description

Analytical data (PXRD, UV−Vis, ^{1}H NMR spectra), crystallographic data (CIF) for **1-4** and $\mathbf{3}_{0.62}$-$\mathbf{4}_{0.38}$, selected bond lengths to determine the major tautomer, photographs of dichroism. CCDC deposition numbers: 1827939-1827943.

Acknowledgements

This work was carried out on XRD equipment from the PC2 platform and on the polarizing microscope from the LOS platform of UNamur. Olivier Deparis is acknowledged for access to the LOS facility of UNamur. Freddy Zutterman, Jean Quartinment, Nicolas Reckinger (Université de Namur), Tom Leyssens, Koen Robeyns and Vanessa Kristina Seiler (Université catholique de Louvain) are gratefully acknowledged for fruitful discussion. A.C. benefits from an F.R.S-FNRS ("Aspirant") grant. S.R.M. was supported by Wallonia-Brussels International (WBI) through a Postdoctoral Fellowship for Excellence program WBI.WORLD and by F.R.S.-FNRS as a Postdoctoral Researcher. This work was published thanks to funding of Actions de Recherche Concertées (ARC) de la Direction générale de l'Enseignement non obligatoire et de la Recherche scientifique—Direction de la Recherche scientifique—Communauté française de Belgique. This work was supported, in part, by the EU COSTAction CM1402 "Crystallize".

References

(1) Zhang, J.; Zou, Q.; Tian, H. Photochromic Materials: More Than Meets The Eye. *Adv. Mater.* **2013**, *25* (3), 378–399.

(2) Kawata, S.; Kawata, Y. Three-Dimensional Optical Data Storage Using Photochromic Materials. *Chem. Rev.* **2000**, *100* (5), 1777–1788.

(3) Cusido, J.; Deniz, E.; Raymo, F. M. Fluorescent Switches Based on Photochromic Compounds. *European J. Org. Chem.* **2009**, *2009* (13), 2031–2045.

(4) Hadjoudis, E.; Mavridis, I. M. Photochromism and Thermochromism of Schiff Bases in the Solid State: Structural Aspects. *Chem. Soc. Rev.* **2004**, *33* (9), 579–588.

(5) Ogawa, K.; Kasahara, Y.; Ohtani, Y.; Harada, J. Crystal Structure Change for the Thermochromy of *N*-Salicylideneanilines. The First Observation by X-Ray Diffraction. *J. Am. Chem. Soc.* **1998**, *120* (28), 7107–7108.

(6) Harada, J.; Uekusa, H.; Ohashi, Y. X-Ray Analysis of Structural Changes in Photochromic Salicylideneaniline Crystals. Solid-State Reaction Induced by Two-Photon Excitation. *J. Am. Chem. Soc.* **1999**, *121* (24), 5809–5810.

(7) Amimoto, K.; Kawato, T. Photochromism of Organic Compounds in the Crystal State. *J. Photochem. Photobiol. C Photochem. Rev.* **2005**, *6* (4), 207–226.

(8) Fukuda, H.; Amimoto, K.; Koyama, H.; Kawato, T. Crystalline Photochromism of N-Salicylidene-2,6-Dialkylanilines: Advantage of 2,6-Dialkyl Substituents of Aniline for Preparation of Photochromic Schiff Base Crystals. *Org. Biomol. Chem.* **2003**, *1* (9), 1578–1583.

(9) Hutchins, K. M.; Dutta, S.; Loren, B. P.; MacGillivray, L. R. Co-Crystals of a Salicylideneaniline: Photochromism Involving Planar Dihedral Angles. *Chem. Mater.* **2014**, *26* (10), 3042–3044.

(10) Staehle, I. O.; Rodríguez-Molina, B.; Khan, S. I.; Garcia-Garibay, M. A. Engineered Photochromism in Crystalline Salicylidene Anilines by Facilitating Rotation to Reach the Colored *Trans*-Keto Form. *Cryst. Growth Des.* **2014**, *14* (7), 3667–3673.

(11) Carletta, A.; Buol, X.; Leyssens, T.; Champagne, B.; Wouters, J. Polymorphic and Isomorphic Cocrystals of a *N*-Salicylidene-3-Aminopyridine with Dicarboxylic Acids: Tuning of Solid-State Photo- and Thermochromism. *J. Phys. Chem. C* **2016**, *120* (18), 10001–10008.

(12) Mercier, G. M.; Robeyns, K.; Leyssens, T. Altering the Photochromic Properties of *N*-

Salicylideneanilines Using a Co-Crystal Engineering Approach. *Cryst. Growth Des.* **2016**, *16* (6), 3198–3205.

(13) Jacquemin, P.-L.; Robeyns, K.; Devillers, M.; Garcia, Y. Photochromism Emergence in *N*-Salicylidene *P* -Aminobenzenesulfonate Diallylammonium Salts. *Chem. - A Eur. J.* **2015**, *21* (18), 6832–6845.

(14) Carletta, A.; Spinelli, F.; d'Agostino, S.; Ventura, B.; Chierotti, M. R.; Gobetto, R.; Wouters, J.; Grepioni, F. Halogen-Bond Effects on the Thermo- and Photochromic Behaviour of Anil-Based Molecular Co-Crystals. *Chem. - A Eur. J.* **2017**, *23* (22), 5317–5329.

(15) Sliwa, M.; Naumov, P.; Choi, H.-J.; Nguyen, Q.-T.; Debus, B.; Delbaere, S.; Ruckebusch, C. Effects of a Self-Assembled Molecular Capsule on the Ultrafast Photodynamics of a Photochromic Salicylideneaniline Guest. *ChemPhysChem* **2011**, *12* (9), 1669–1672.

(16) Jacquemin, P.-L.; Robeyns, K.; Devillers, M.; Garcia, Y. Reversible Photochromism of an *N*-Salicylidene Aniline Anion. *Chem. Commun.* **2014**, *50* (6), 649–651.

(17) Yamazaki, Y.; Sekine, A.; Uekusa, H. In Situ Control of Photochromic Behavior through Dual Photo-Isomerization Using Cobaloxime Complexes with Salicylidene-3-Aminopyridine and 3-Cyanopropyl Ligands. *Cryst. Growth Des.* **2017**, *17* (1), 19–27.

(18) Robert, F.; Naik, A. D.; Tinant, B.; Robiette, R.; Garcia, Y. Insights into the Origin of Solid-State Photochromism and Thermochromism of *N*-Salicylideneanils: The Intriguing Case of Aminopyridines. *Chem. - A Eur. J.* **2009**, *15* (17), 4327–4342.

(19) Houjou, H.; Ikedo, H.; Yoshikawa, I. Single-Crystal UV-Vis Spectroscopic Examination of a Striking Odd–Even Effect on Structure and Chromic Behaviour of Salicylidene Alkylamines. *Chem. Commun.* **2017**, *53* (79), 10898–10901.

(20) Quertinmont, J.; Carletta, A.; Tumanov, N. A.; Leyssens, T.; Wouters, J.; Champagne, B. Assessing Density Functional Theory Approaches for Predicting the Structure and Relative Energy of Salicylideneaniline Molecular Switches in the Solid State. *J. Phys. Chem. C* **2017**, *121* (12), 6898–6908.

(21) Christopherson, J.-C.; Topić, F.; Barrett, C. J.; Friščić, T. Halogen-Bonded Cocrystals as Optical Materials: Next-Generation Control over Light–Matter Interactions. *Cryst. Growth Des.* **2018**, *18* (2), 1245–1259.

(22) d'Agostino, S.; Grepioni, F.; Braga, D.; Ventura, B. Tipping the Balance with the Aid of Stoichiometry: Room Temperature Phosphorescence versus Fluorescence in Organic Cocrystals. *Cryst. Growth Des.* **2015**, *15* (4), 2039–2045.

(23) Wang, H.; Hu, R. X.; Pang, X.; Gao, H. Y.; Jin, W. J. The Phosphorescent Co-Crystals of 1,4-Diiodotetrafluorobenzene and Bent 3-Ring-*N*-Heterocyclic Hydrocarbons by C-I···N and C-I···π Halogen Bonds. *CrystEngComm* **2014**, *16* (34), 7942–7948.

(24) Xu, J.; Liu, X.; Ng, J. K.-P.; Lin, T.; He, C. Trimeric Supramolecular Liquid Crystals Induced by Halogen Bonds. *J. Mater. Chem.* **2006**, *16* (35), 3540–3545.

(25) Bushuyev, O. S.; Friščić, T.; Barrett, C. J. Controlling Dichroism of Molecular Crystals by Cocrystallization. *Cryst. Growth Des.* **2016**, *16* (2), 541–545.

(26) Cinčić, D.; Friščić, T.; Jones, W. Isostructural Materials Achieved by Using Structurally Equivalent Donors and Acceptors in Halogen-Bonded Cocrystals. *Chem. - A Eur. J.* **2008**, *14* (2), 747–753.

(27) Cinčić, D.; Friščić, T.; Jones, W. A Cocrystallisation-Based Strategy to Construct Isostructural Solids. *New J. Chem.* **2008**, *32* (10), 1776–1781.

(28) Cinčić, D.; Friščić, T.; Jones, W. Structural Equivalence of Br and I Halogen Bonds: A Route to Isostructural Materials with Controllable Properties. *Chem. Mater.* **2008**, *20* (21), 6623–6626.

(29) Marabello, D.; Antoniotti, P.; Benzi, P.; Canepa, C.; Mortati, L.; Sassi, M. P.; IUCr. Synthesis, Structure and Non-Linear Optical Properties of New Isostructural *β*-D-Fructopyranose Alkaline Halide Metal–organic Frameworks: A Theoretical and an Experimental Study. *Acta Crystallogr. Sect. B Struct. Sci. Cryst. Eng. Mater.* **2017**, *73* (4), 737–743.

(30) Zhang, W.-L.; He, Z.-Z.; Xia, T.-L.; Luo, Z.-Z.; Zhang, H.; Lin, C.-S.; Cheng, W.-D. Syntheses and Magnetic Properties Study of Isostructural $BiM_2BP_2O_{10}$ (M = Co, Ni) Containing a Quasi-1D Linear Chain Structure. *Inorg. Chem.* **2012**, *51* (16), 8842–8847.

(31) Hutchins, K. M.; Unruh, D. K.; Verdu, F. A.; Groeneman, R. H. Molecular Pedal Motion Influences Thermal Expansion Properties within Isostructural Hydrogen-Bonded Co-Crystals. *Cryst. Growth Des.* **2018**, *18* (2), 566–570.

(32) Kitaigorodskii, A. I. *Mixed Crystals*; Springer-Verlag: Berlin, 1984.

(33) Cruz-Cabeza, A. J.; Lestari, M.; Lusi, M. Cocrystals Help Break the "Rules" of Isostructurality: Solid Solutions and Polymorphism in the Malic/Tartaric Acid System. *Cryst. Growth Des.* **2018**, *18* (2), 855–863.

(34) Lusi, M.; Vitorica-Yrezabal, I. J.; Zaworotko, M. J. Expanding the Scope of Molecular Mixed Crystals Enabled by Three Component Solid Solutions. *Cryst. Growth Des.* **2015**, *15* (8), 4098–4103.

(35) Weerasekara, R. K.; Uekusa, H.; Hettiarachchi, C. V. Multicolor Photochromism of Fulgide Mixed Crystals with Enhanced Fatigue Resistance. *Cryst. Growth Des.* **2017**, *17* (6), 3040–3047.

(36) James, S. L.; Adams, C. J.; Bolm, C.; Braga, D.; Collier, P.; Friščić, T.; Grepioni, F.; Harris, K. D. M.; Hyett, G.; Jones, W.; et al. Mechanochemistry: Opportunities for New and Cleaner Synthesis. *Chem. Soc. Rev.* **2012**, *41* (1), 413–447.

(37) Zbačnik, M.; Kaitner, B. Ex Situ and in Situ Monitoring of the Syntheses of Thermochromic Schiff Bases. *CrystEngComm* **2014**, *16* (20), 4162.

(38) Carletta, A.; Dubois, J.; Tilborg, A.; Wouters, J. Solid-State Investigation on a New Dimorphic Substituted N-Salicylidene Compound: Insights into Its Thermochromic Behaviour. *CrystEngComm* **2015**, *17* (18), 3509–3518.

(39) Sheldrick, G. M. SHELXT – Integrated Space-Group and Crystal-Structure Determination. *Acta Crystallogr. Sect. A Found. Adv.* **2015**, *71* (1), 3–8.

(40) Sheldrick, G. M. Crystal Structure Refinement with SHELXL. *Acta Crystallogr. Sect. C, Struct. Chem.* **2015**, *71* (Pt 1), 3.

(41) Macrae, C. F.; Edgington, P. R.; McCabe, P.; Pidcock, E.; Shields, G. P.; Taylor, R.; Towler, M.; van de Streek, J. Mercury : Visualization and Analysis of Crystal Structures. *J. Appl. Crystallogr.* **2006**, *39* (3), 453–457.

(42) Gates, B. C.; Knözinger, H.; Jentoft, F. C. *Advances in Catalysis Vol. 52*; Academic Press, 2009.

(43) Johmoto, K.; Sekine, A.; Uekusa, H. Photochromism Control of Salicylideneaniline Derivatives by Acid–Base Co-Crystallization. *Cryst. Growth Des.* **2012**, *12* (10), 4779–4786.

(44) Avadanei, M.; Cozan, V.; Shova, S.; Paixao, J. A. Solid State Photochromism and Thermochromism of Two Related N-Salicylidene Anilines. *Chem. Phys.* **2014**, *444*, 43–51.

(45) Minemawari, H.; Tanaka, M.; Tsuzuki, S.; Inoue, S.; Yamada, T.; Kumai, R.; Shimoi, Y.; Hasegawa, T. Enhanced Layered-Herringbone Packing due to Long Alkyl Chain Substitution in Solution-Processable Organic Semiconductors. *Chem. Mater.* **2017**, *29* (3), 1245–1254.

(46) Childs, S. L.; Wood, P. A.; Rodríguez-Hornedo, N.; Reddy, L. S.; Hardcastle, K. I. Analysis of 50 Crystal Structures Containing Carbamazepine Using the *Materials* Module of *Mercury CSD*. *Cryst. Growth Des.* **2009**, *9* (4), 1869–1888.

(47) Denton, A. R.; Ashcroft, N. W. Vegard's Law. *Phys. Rev. A* **1991**, *43* (6), 3161–3164.

(48) Dean, P. A. W.; Jennings, M.; Rajalingam, U.; Craig, D. C.; Scudder, M. L.; Dance, I. G. The Crystal Packing of $[Cd(C_4H_8N_2S)_4](BPh_4)_2 \cdot 2MeCN$ and $[Cd(C_4H_8N_2S)_4](CF_3SO_3)_2$. Tetraphenylborate Forming an Aryl Box. *CrystEngComm* **2002**, *4* (9), 46–50.

(49) Schur, E.; Nauha, E.; Lusi, M.; Bernstein, J. Kitaigorodsky Revisited: Polymorphism and Mixed Crystals of Acridine/Phenazine. *Chem. - A Eur. J.* **2015**, *21* (4), 1735–1742.

(50) Harada, J.; Ogawa, K. Pedal Motion in Crystals. *Chem. Soc. Rev.* **2009**, *38* (8), 2244.

(51) Sliwa, M.; Létard, S.; Malfant, I.; Nierlich, M.; Lacroix, P. G.; Asahi, T.; Masuhara, H.; Yu, P.; Nakatani, K. Design, Synthesis, Structural and Nonlinear Optical Properties of Photochromic Crystals: Toward Reversible Molecular Switches. *Chem. Mater.* **2005**, *17*, 4727–4735.

(52) Christopherson, J.-C.; Potts, K. P.; Bushuyev, O. S.; Topić, F.; Huskić, I.; Rissanen, K.; Barrett, C. J.; Friščić, T. Assembly and Dichroism of a Four-Component Halogen-Bonded Metal–Organic Cocrystal Salt Solvate Involving Dicyanoaurate(I) Acceptors. *Faraday Discuss.* **2017**, *203*, 441–457.

(53) Braga, D. Crystal Engineering, Where from? Where to? *Chem. Commun.* **2003**, *108* (22), 2751–2754.

(54) Desiraju, G. R. Crystal Engineering: a Holistic View. *Angew. Chemie Int. Ed.* **2007**, *46* (44), 8342–8356.

TOC GRAPHIC

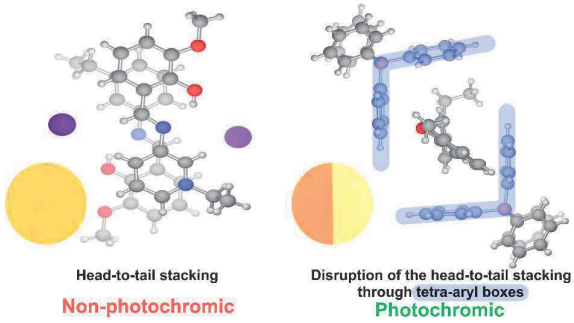
Head-to-tail stacking
Non-photochromic
Disruption of the head-to-tail stacking
through tetra-aryl boxes
Photochromic